

## Folding model analysis of 240 MeV ${}^6\text{Li}$ elastic scattering on ${}^{116}\text{Sn}$ and inelastic scattering to low-lying states of ${}^{116}\text{Sn}$

X. Chen, Y.-W. Lui, H. L. Clark, Y. Tokimoto, and D. H. Youngblood  
*Cyclotron Institute, Texas A&M University, College Station, Texas 77843, USA*  
 (Received 20 July 2007; published 21 November 2007)

Elastic scattering of 240 MeV  ${}^6\text{Li}$  ions from  ${}^{116}\text{Sn}$  was measured from  $4^\circ \leq \theta_{\text{c.m.}} \leq 32^\circ$ . The data were fitted with a Woods-Saxon phenomenological potential and with double folding models using the  $M3Y NN$  effective interaction with and without density dependence. DWBA calculations with the fitted parameters were used to calculate cross sections for inelastic scattering to low-lying  $2^+$  and  $3^-$  states.  $B(E2)$  and  $B(E3)$  values were extracted and compared with electromagnetic values and those obtained from  $\alpha$  inelastic scattering.

DOI: [10.1103/PhysRevC.76.054606](https://doi.org/10.1103/PhysRevC.76.054606)

PACS number(s): 25.70.Bc, 24.10.Ht, 27.60.+j

### I. INTRODUCTION

Alpha inelastic scattering at small angles has been widely and successfully used to study the isoscalar giant monopole resonance (ISGMR) in many stable medium and heavy nuclei [1]. For light nuclei ( $A < 40$ ), ISGMR strengths are fragmented and extend to excitation energies above 35 MeV. However, the large physical background at high excitation energy in  $\alpha$  inelastic scattering, due to multistep reactions, makes it difficult to extract strengths in this range.  ${}^6\text{Li}$  inelastic scattering could be an alternate tool to study the ISGMR in this region, because  ${}^6\text{Li}$  scattering has a low particle emitting threshold, which means physical background due to multistep processes is low, especially at higher excitation energy. A study of  ${}^6\text{Li}$  elastic scattering is necessary because the optical parameters obtained from elastic scattering will be used to analyze inelastic scattering.

${}^6\text{Li}$  elastic scattering itself is very interesting. Although elastic scattering is the simplest hadron induced nuclear reaction, it carries important information about nuclear properties. The optical model (OM) has been widely used to analyze heavy ion scattering data in terms of empirical Woods-Saxon (WS) parametrizations of the nuclear potential. However, it was found that a satisfactory microscopic understanding of heavy ion scattering can be obtained if one relates the optical potential to a fundamental nucleon-nucleon ( $NN$ ) interaction. Double folding (DF) does this by folding the interaction with the nuclear matter densities of both the target and projectile nuclei [2]. During the last several decades, a diverse assortment of heavy ion scattering studies have been carried out with considerable success using the DF model (see [3] and references therein). However, in studies of the elastic scattering of  ${}^6\text{Li}$ , it has been found that the magnitude of the folded potential must be reduced by a renormalization factor  $N_R \sim 0.5\text{--}0.6$  to fit the data. Since  ${}^6\text{Li}$  is loosely bound, it is thought that the breakup of the projectile is responsible for the substantial renormalization. This effect can be represented by a complex dynamical polarization potential (DPP) which has a strongly repulsive real part. By using coupled discretized continuum channels (CDCC) techniques, Sakuragi *et al.* [4–6] confirmed that the elastic scattering data could be fitted well with the potential renormalization close to unity when coupling to breakup channel was included.  ${}^6\text{Li}$  is in the mass number

range  $A = 4\text{--}12$ , where the elastic scattering shows a transition between characteristics of light ions ( $A \leq 4$ ) and characteristics of heavy ion ( $A \geq 12$ ). Such data could provide a stronger test of the validity of any model for heavy ion potentials [7,8].

The  ${}^6\text{Li}$  elastic scattering from various targets has been extensively studied with bombarding energies below 200 MeV [7,9–14] during 1970's to 1980's. From 1988 to 1993, Nadasen *et al.* reported a series of systematic studies [15–17] of  ${}^6\text{Li}$  scattering off of  ${}^{12}\text{C}$ ,  ${}^{28}\text{Si}$ ,  ${}^{40}\text{Ca}$ ,  ${}^{58}\text{Ni}$ ,  ${}^{90}\text{Zr}$ ,  ${}^{208}\text{Pb}$  at 210 MeV and off of  ${}^{12}\text{C}$ ,  ${}^{28}\text{Si}$  at 318 MeV with phenomenological and folding-model potentials. A study of 600 MeV  ${}^6\text{Li}$  scattering on  ${}^{12}\text{C}$ ,  ${}^{58}\text{Ni}$ ,  ${}^{90}\text{Zr}$ , and  ${}^{208}\text{Pb}$  targets [18] was reported in 2000 investigating the coupling-effect between the elastic and the breakup channels at intermediate energy.

In this work, 240 MeV  ${}^6\text{Li}$  elastic scattering on  ${}^{116}\text{Sn}$  was carried out and the optical potential model was used to fit the data. Both WS model and double folding models were used to construct the real part of the optical potential, while the imaginary part of the potential was represented by a WS phenomenological shape. The differential cross sections for the low-lying  $2^+$  state at 1.29 MeV and  $3^-$  state at 2.27 MeV were also extracted from the experiment. DWBA calculations for these states were carried out and the best fit values for  $B(EL)$  with all the models were extracted.

### II. EXPERIMENTAL TECHNIQUE AND RESULTS

The experimental technique for the  ${}^6\text{Li}$  scattering measurements was similar to that for  $\alpha$  scattering which has been described in Ref. [19] and is summarized briefly below. A beam of 240 MeV  ${}^6\text{Li}$  particles from the Texas A&M University K500 superconducting cyclotron passed through a beam analysis system [20] and bombarded a self-supporting 9.9 mg/cm<sup>2</sup> Sn foil which was enriched to 95% in  ${}^{116}\text{Sn}$  and located in the target chamber of the multipole-dipole-multipole spectrometer (MDM) [21]. The horizontal acceptance of the spectrometer was  $4^\circ$  and ray tracing was used to reconstruct the scattering angle. The vertical acceptance was set at  $\pm 1^\circ$  for spectrometer angles from  $5^\circ$  to  $9^\circ$  and  $\pm 2^\circ$  for spectrometer angles from  $11^\circ$  to  $32^\circ$ . The outgoing particles were detected by a 60 cm long focal plane detector. The principles of operation of the detector are similar to the detector described

in Ref. [22]. It contains four proportional counters to measure position, as well as an ionization chamber to provide  $\Delta E$  and a scintillator behind the ionization chamber to measure the energy deposited and provide a fast timing signal for each event. The out-of-plane scattering angle was not measured. The details of angle and position calibrations were described in Ref. [23]. Position resolution of approximately 0.9 mm and scattering angle resolution of about  $0.09^\circ$  were obtained.

In the data analysis, data taken at one spectrometer angle was divided into ten angle bins, with each angle bin corresponding to  $\Delta\theta \approx 0.4^\circ$ . The average angle for each angle bin was determined by integrating over the height of the solid angle and the width of the angle bin. The target thickness was obtained by measuring the energy loss of a 240 MeV  $\alpha$  beam passing through the target. The absolute differential cross-section for each angle bin was obtained from the combination of yield, charge integration, target thickness, solid angle, and dead time correction. The cumulative uncertainties in target thickness, solid angle, etc., result in a  $\pm 10\%$  uncertainty in cross section.

### III. OPTICAL MODEL AND FOLDED POTENTIAL

#### A. Optical potential and deformed potential model

The phenomenological WS potential has been widely used to describe elastic scattering and the parameters are obtained by fitting elastic scattering data. The transition potential used to describe inelastic scattering to excited states of the target nucleus is directly obtained as the derivative of the WS potential  $U(r)$  for  $\ell \geq 2$ . In the deformed potential model (DP), excitations of the nucleus with multipolarity  $\ell \geq 2$  are characterized by a transition potential whose shape is independent of  $\ell$ :

$$G_\ell^{\text{DP}}(r) = -\delta_\ell^U \frac{dU(r)}{dr}, \quad (1)$$

where  $\delta_\ell^U$  is the potential deformation length. Since the nuclear interaction is short range, it is assumed that the interaction potential  $U(r)$  between an incident projectile and the target nucleus undergoes oscillations in shape that follow the density motion [24] and that the deformation lengths for the potential are the same as those for density, i.e.,  $\delta_\ell^U = \delta_\ell^m$ . However, Beene *et al.* [25] have shown that a consistent agreement between electromagnetic transition strengths and those measured with light- and heavy-ion inelastic scattering for low-lying  $2^+$  and  $3^-$  states can only be obtained using the folding model.

#### B. Folding model

An alternate way to construct the optical and transition potentials is to fold the  $NN$  effective interaction over the densities and transition densities of target and projectile. The transition density for the excited nucleus was constructed with Bohr-Mottelson (BM) collective model described by Satchler [24]. With the first order approximation, the transition density for  $\ell \geq 2$  can be expressed as

$$g_\ell = -\delta_\ell^m \frac{d\rho(r)}{dr}, \quad (2)$$

where  $\rho(r)$  is the ground state density of the excited nucleus and  $\delta_\ell^m$  is the corresponding matter deformation length. There are several nucleon-nucleon effective interactions which have been used in the folding model, such as the JLM interaction [26], the S1Y interaction [8,27] and the M3Y interaction. The M3Y interaction was used to construct the folded potentials in this work.

There are two versions of M3Y  $NN$  interactions, the M3Y-Reid  $NN$  interaction [28] and M3Y-Paris effective  $NN$  interaction [29]. The spin- and isospin-independent central terms of the two M3Y interactions can be expressed as

$$\begin{aligned} \text{M3Y - Reid : } v_{00}(r) &= \left[ 7999 \frac{e^{-4r}}{4r} - 2134 \frac{e^{-2.5r}}{2.5r} \right] \text{ MeV,} \\ \text{M3Y - Paris : } v_{00}(r) &= \left[ 11062 \frac{e^{-4r}}{4r} - 2538 \frac{e^{-2.5r}}{2.5r} \right] \text{ MeV.} \end{aligned} \quad (3)$$

There are two ways to estimate the knock-on exchange contribution for each version. One way is to use a delta function where the strength  $J_{00}(E)$  [30] can be expressed as [2,3]

$$\begin{aligned} \text{M3Y - Reid : } \hat{J}_{00}(E) &\approx -276[1 - 0.005(E/A)] \text{ MeVfm}^3, \\ \text{M3Y - Paris : } \hat{J}_{00}(E) &\approx -590[1 - 0.002(E/A)] \text{ MeVfm}^3, \end{aligned} \quad (4)$$

and where  $E/A$  is the bombarding energy per projectile nucleon. Another way is to use the finite range approximation, in which the knock-on exchange effect is expressed as a sum of three Yukawa terms which represent the long-range one pion exchange, medium range multiple-pion exchange and a short range interaction. The knock-on exchange contributions can be expressed as

$$\begin{aligned} \text{M3Y - Reid : } \hat{v}_{00}(r) &= \left[ 4631 \frac{e^{-4r}}{4r} - 1787 \frac{e^{-2.5r}}{2.5r} - 7.847 \frac{e^{-0.7072r}}{0.7072r} \right] \text{ MeV,} \\ \text{M3Y - Paris : } \hat{v}_{00}(r) &= \left[ -1524 \frac{e^{-4r}}{4r} - 518.8 \frac{e^{-2.5r}}{2.5} - 7.847 \frac{e^{-0.7072r}}{0.7072r} \right] \text{ MeV.} \end{aligned} \quad (5)$$

A density dependent M3Y effective  $NN$  interaction has been discussed in detail by Khoa *et al.* [31–33]. Generally the density dependent  $NN$  interaction is assumed to have the separable form

$$v_{D(EX)}(\rho, r) = F(\rho)v_{D(EX)}(r), \quad (6)$$

where  $F(\rho)$  is density dependent function. The CDM3Yn [32] is used in this work and  $F(\rho)$  is expressed as following:

$$F(\rho) = C[1 + \alpha \exp(-\beta\rho) - \gamma\rho], \quad (7)$$

where  $C, \alpha, \beta, \gamma$  are parameters chosen for different density dependent functions.

### IV. DATA ANALYSIS AND DISCUSSION

Elastic scattering data were fitted by the WS phenomenological potential model and potentials derived from double folding. Fermi distributions obtained from droplet model

TABLE I. Density parameters for the folding calculations. Fermi parameters  $c$  (half density radius) and  $a$  (diffuseness) are given for the matter distribution.  $R_m$  and  $R_{\text{Coul}}$  stand for mean square root radii for matter distribution and Coulomb interaction, respectively.

Model	Density form	Nucleus	$C$ (fm)	$A$ (fm)	$R_m$ (fm)	$R_{\text{Coul}}$ (fm)
DIF	Fermi [34]	${}^6\text{Li}$	1.508	0.5	2.195	2.195
	Fermi [34]	${}^{116}\text{Sn}$	5.469	0.5	4.626	4.626
DDF	COSMA [36]	${}^6\text{Li}$	–	–	2.444	1.833 <sup>a</sup>
	Fermi [35]	${}^{116}\text{Sn}$	5.49	0.515	4.663	4.253 <sup>a</sup>

<sup>a</sup>Uniform charge distribution is used in the calculations to estimate the Coulomb interaction for elastic scattering.

calculations [34] were used for target and projectile density in the density independent folding (DIF) calculation. In the density dependent folding (DDF) calculation, a Fermi distribution was used for the ground state of  ${}^{116}\text{Sn}$ , with the parameters obtained from Ref. [35], and the  ${}^6\text{Li}$  ground state density was obtained from proton scattering with the cluster-orbital shell-model approximation (COSMA) [36]. The proton and the neutron densities of  ${}^6\text{Li}$  were expressed as

$$\rho_{n,p} = N_c \frac{\exp(-r^2/a^2)}{\pi^{3/2}a^3} + N_v \frac{2 \exp(-r^2/b^2)}{3\pi^{3/2}b^5} \times \left[ Ar^2 + B \left( r^2 - \frac{3}{2}b^2 \right)^2 \right], \quad (8)$$

where  $N_c = 2.0$ ,  $N_v = 1.0$ ,  $a = 1.55$ ,  $b = 2.07$ ,  $A = 1.0$  and  $B = 0.0$ . The density parameters used in the folding calculations are listed in Table I.

Elastic scattering fits with WS phenomenological potentials were carried out with ECIS [37]. The WS potential has the 3-parameter form

$$V(r) = V/[1 + \exp((r - R_V)/a)], \quad (9)$$

$$R_V = r_0(A_T^{1/3} + A_p^{1/3}),$$

where  $A_T$  is the mass number of the target and  $A_p$  is the mass number of projectile. The real and imaginary parts have the same form except the parameter values are different.

Satchler and Khoa [38] found that better fits to the measurements taken at angles beyond the Fraunhofer diffraction region were obtained by a hybrid model in which the real interaction was obtained with folding and the imaginary part

was represented by a Woods-Saxon potential. So in this work, only the real parts of the optical potentials were obtained by a folding procedure with both the DIF model and the DDF model. The DDF folding calculations were carried out with the folding code DFPD4 [39], while the DIF calculations were carried out with CHEN2 [34], and the differential cross sections were obtained with ECIS. In the DIF calculation, the Reid version of the M3Y  $NN$  interaction was used and the knock-on exchange contribution was represented by zero-range approximation which is a  $\delta$  function with strength shown in Eq. (4). In the DDF calculation, the Paris version M3Y  $NN$  interaction was used and the knock-on exchange effect was represented by a finite range approximation shown in Eq. (5). The density dependent function is expressed as [32]

$$F(\rho) = 0.2658(1 + 3.8033e^{-1.4099\rho} - 4.0\rho). \quad (10)$$

There is also a weak energy dependence included in the density dependent  $NN$  effective interaction, which is used to reproduce the empirical energy dependence of the nucleon-nucleus optical potential [31] and is expressed as following:

$$g(\varepsilon) \approx 1 - 0.003 \varepsilon \quad (11)$$

where  $\varepsilon$  is the bombarding energy per nucleon (in MeV). The direct term and exchange term of the  $NN$  effective interaction in DDF calculation thus are expressed as

$$v_{D(EX)}(\rho, \varepsilon, r) = g(\varepsilon)F(\rho)v_{D(EX)}(r). \quad (12)$$

The optical potential parameter sets obtained from both folding model fits as well as the WS fit are listed in Table II. The calculated angular distributions for the ratio between

TABLE II. Optical parameters sets obtained from the analysis of  ${}^6\text{Li}$  scattering. WS means Woods-Saxon potential. DIF means density independent folded potential and DDF means density dependent folded potential. The asterisk means that  $R_{v(w)} = r_{0(i0)}A_T^{1/3}$ .

$E_{\text{Li}}$ (MeV)	Target	Potential type	$N_R$	$V$ (MeV)	$r_0$ (fm)	$A$ (fm)	$W$ (MeV)	$r_{10}$ (fm)	$a_I$ (fm)	$J_v$ (MeV fm <sup>3</sup> )	$J_w$ (MeV fm <sup>3</sup> )	$\chi^2$	$\sigma_r$ (mb)
240	${}^{116}\text{Sn}$	WS		195.9	0.825	0.934	27.98	1.178	0.823	254.3	91.4	0.77	2885
		DIF	0.637				39.99	1.075	0.992	234.4	106.4	1.19	3031
		DDF	0.659				28.77	1.151	0.905	202.1	89.9	0.98	2956
210 [8]	${}^{90}\text{Zr}$	WS		177	1.182*	0.939	31.30	1.627*	0.810	257.0	106.0	8.3	2618
		DIF	0.70				31.30	1.596*	0.917	263.0	103.0	4.9	2744
	${}^{208}\text{Pb}$	WS		224.0	1.104*	1.001	35.10	1.518*	0.824	259.0	93.0	0.6	3536
		DIF	0.60				31.40	1.537*	0.842	224.0	86.0	1.8	3582

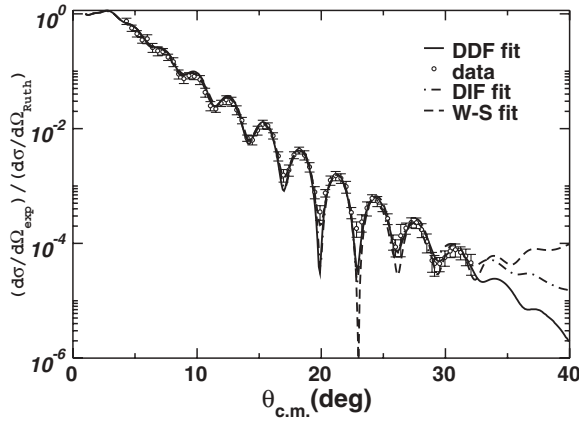


FIG. 1. Experimental angular distribution of the cross section (relative to Rutherford cross section) and fits for  ${}^6\text{Li}+{}^{116}\text{Sn}$  elastic scattering using WS potential, DIF potential and DDF potential parameters are shown. The error bars indicate statistical and systematic errors.

absolute differential nuclear cross section and Rutherford cross section are plotted along with elastic scattering data in Fig. 1. The renormalization factors in both folding calculation are around 0.65, consistent with earlier folding analysis of  ${}^6\text{Li}$  scattering [2,8]. The real parts of the potentials obtained from the different models are plotted in Fig. 2, where the folded potentials are multiplied by the renormalization factor  $N_R$  obtained from the fits of elastic scattering data. The amplitudes of the potentials are quite different for smaller radii, however they overlap well for radii in the surface region ( $R \sim 7.4$  fm is roughly the sum of radii of the projectile and target), indicating that peripheral collisions dominate in the angular range studied here. From Fig. 1 it is apparent that even an additional  $10^\circ$  (out to  $40^\circ$ ) could have improved the parameterization and such larger angles measurements would help to determine the amplitude of interior potential.

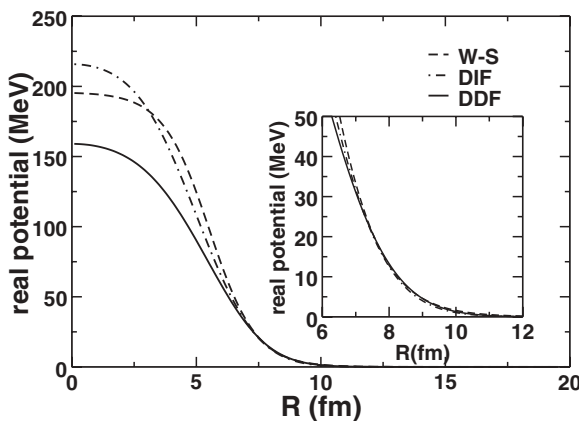


FIG. 2. Real optical potentials obtained from WS, DIF, DDF models. For DIF model, the dash and dot curve shows the folded potential obtained from CHEN2 multiplied by renormalization factor  $N_R = 0.637$ . For DDF model, the black curve shows the folded potential obtained from DFPD4 multiplied by renormalization factor  $N_R = 0.659$ . The inset has the vertical scale expanded to show the region of overlap.

The quality of fit of elastic scattering and inelastic scattering to low-lying  $2^+$  and  $3^-$  states is estimated by  $\chi^2$ , defined by

$$\chi^2 = \frac{1}{N} \sum_{i=1}^N \left[ \frac{\sigma(\theta_i)^{\text{cal}} - \sigma(\theta_i)^{\text{exp}}}{\Delta\sigma(\theta_i)} \right]^2 \quad (13)$$

where  $N$  is the number of data points,  $\sigma(\theta_i)^{\text{cal}}$  is the  $i$ th calculated cross section,  $\sigma(\theta_i)^{\text{exp}}$  is the experimental cross section, and  $\Delta\sigma(\theta_i)$  is the corresponding absolute uncertainty.  $\chi^2$  obtained from WS model fit has no significant difference with those obtained from folding model fits. Since there have been no  ${}^6\text{Li}+{}^{116}\text{Sn}$  scattering data reported before, the optical parameters sets from Ref. [8] for 210 MeV  ${}^6\text{Li}$  scattering on  ${}^{90}\text{Zr}$  and  ${}^{208}\text{Pb}$  are also shown in Table II for comparison. Farid and Hassanain [8] obtained their  $\chi^2$  assuming the  ${}^{90}\text{Zr}$  and  ${}^{208}\text{Pb}$  data have uniform 10% error. In order to compare the fit for  ${}^{90}\text{Zr}$  and our  ${}^{116}\text{Sn}$ ,  $\chi^2$  as recalculated for  ${}^{116}\text{Sn}$  by assuming the data have 10% uncertainty. The calculations show that WS model fit for  ${}^{116}\text{Sn}$  data ( $\chi^2 \sim 5.16$ ) is better than the WS fit for  ${}^{90}\text{Zr}$  data ( $\chi^2 \sim 8.3$ ), while fits with double folding models for  ${}^{116}\text{Sn}$  ( $\chi^2 \sim 5.18$ ) and  ${}^{90}\text{Zr}$  ( $\chi^2 \sim 4.9$ ) have approximately the same quality.

The volume integral of optical potentials per interacting nucleon pair were determined by the relation

$$J_{V,W} = \frac{1}{A_T A_P} \int V(r), W(r) d\tau, \quad (14)$$

where  $V(r)$  and  $W(r)$  are the real and imaginary parts of the optical potential and  $A_T$  and  $A_P$  are the mass numbers of the target and projectile. Based on folding model analysis of light HI elastic scattering with density independent S1Y  $NN$  interaction at intermediate energy [27], Satchler obtained a qualitative expression for the volume integral per nucleon pair with linear energy dependence:

$$J_V^{S1Y} = -259(1 - 0.005E/A_P), \quad (15)$$

where  $E$  is the incident energy and  $A_P$  is the mass of the projectile. For 240 MeV  ${}^6\text{Li}$  scattering,  $J_V^{S1Y} = 207 \text{ MeV fm}^3$ . Even earlier, Gupta and Murthy [40] proposed a semi-empirical formula for the real volume integrals based on nucleon-nucleus optical potential derived from the JLM interaction. The volume integral given by the semi-empirical formula is both energy dependent and target mass dependent. The value of volume integral will slowly decrease as the incident energy and target mass increase. For 240 MeV  ${}^6\text{Li}$  scattering on  ${}^{116}\text{Sn}$ ,  $J_V^{\text{JLM}} = 217 \text{ MeV fm}^3$ . On the other hand, Nadasen *et al.* [16] analyzed 210 MeV  ${}^6\text{Li}$  scattering on  ${}^{90}\text{Zr}$  with WS potential model and suggested an empirical logarithmic energy dependence form for the volume integral per nucleon pair:

$$J_V^{WS} = J_0 - \beta \ln E, \quad (16)$$

where  $J_0 = 855 \pm 30 \text{ MeV fm}^3$ ,  $\beta = 113 \pm 5 \text{ MeV fm}^3$ , and  $E$  is the incident energy of the projectile. For 240 MeV  ${}^6\text{Li}$  scattering,  $J_V^{WS} = 236 \text{ MeV fm}^3$ .

These are compared with those obtained in this experiment in Fig. 3. The volume integral obtained with WS potential model and DIF model are close to the calculation based on

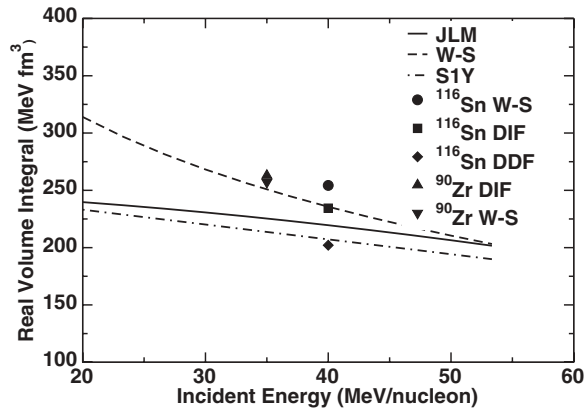


FIG. 3. The volume integral for real part of optical potential obtained with WS model, DIF model and DDF model. The curves with dash, black, dash and dot represent Nadasen *et al.*'s expression obtained with WS potential [16], Gupta and Murthy's expression obtained with JLM effective interaction [40] and Satchler's expression obtained with S1Y effective  $NN$  interaction [27], respectively. Volume integrals obtained from Ref. [8] for 210 MeV  ${}^6\text{Li}$  scattering on  ${}^{90}\text{Zr}$  are also plotted in the figure for comparison.

Nadasen *et al.*'s formula, while DDF calculation is closer to Satchler's expression and Gupta and Murthy's expression. The volume integral per nucleon pair for 240 MeV  ${}^6\text{Li}$  scattering on  ${}^{116}\text{Sn}$  should be slightly smaller than that of 210 MeV  ${}^6\text{Li}$  scattering on  ${}^{90}\text{Zr}$  because it has a higher incident energy and a heavier target and that is seen for both the WS model and folding model calculations.

The DWBA calculations with deformed potential model and folding models for low-lying  $2^+$  and  $3^-$  states of  ${}^{116}\text{Sn}$  were carried out with ECIS. The angular distributions of the cross sections with different models for  $2^+$  and  $3^-$  states are plotted in Figs. 4 and 5 along with the data. For the folding model calculations, the mass deformation length and coulomb deformation length were assumed to be the same,

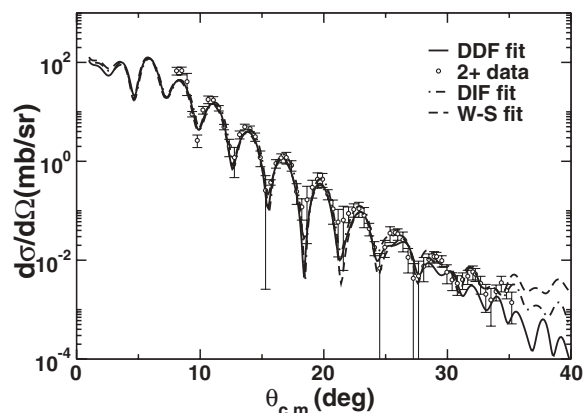


FIG. 4. The differential cross-sections calculated with deformed potential model and folding models for inelastic scattering to the 1.29 MeV  $2^+$  state of  ${}^{116}\text{Sn}$  along with the data points are plotted versus average center of mass angle. The  $B(E2)$  values used for DP, DIF, and DDF models calculations are best fit values of 0.229, 0.182,  $0.233e^2b^2$  respectively. The error bars represent statistical and systematic errors.

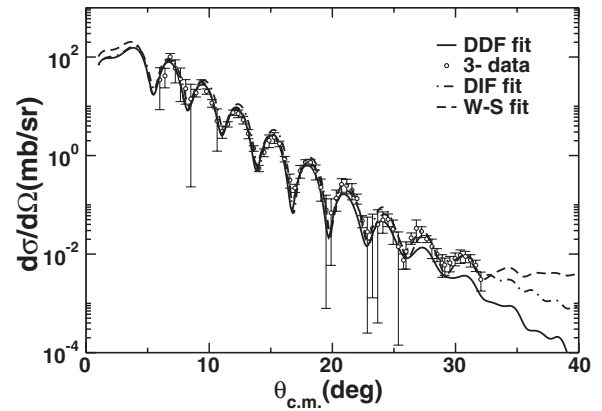


FIG. 5. The differential cross-sections calculated with deformed potential model and folding models for inelastic scattering to the 2.27 MeV  $3^-$  state of  ${}^{116}\text{Sn}$  along with the data points are plotted versus average center of mass angle. The  $B(E3)$  value used for DP, DIF, and DDF models calculations are best fit values of 0.116, 0.101,  $0.133e^2b^3$  respectively. The error bars represent statistical and systematic errors.

and in deformed potential model calculations the potential deformation length and coulomb deformation length were assumed to be the same. In DIF model calculation, the real transition potentials for  $2^+$  and  $3^-$  states were generated with CHEN2 and the imaginary part was obtained by the DP model, while in the DDF calculation, the real transition potentials were generated by DFPD4 and the imaginary parts were obtained by DP model. The best fit  $B(EL)$  values for  $2^+$  and  $3^-$  states with different model calculations were extracted by fitting the inelastic scattering cross section and are listed in Table III.

TABLE III. The best fit  $B(EL)$  value for  $2^+$  and  $3^-$  states of  ${}^{116}\text{Sn}$  obtained with WS, DIF and DDF models. Adopted values of  $B(E2)$  and  $B(E3)$ , as well as values extracted from  $\alpha$  inelastic scattering and from electron scattering, are shown in the table. For  $B(EL)$  values obtained from  ${}^6\text{Li}$  scattering, the superscript errors represent statistical errors, while the subscript errors represent total errors including statistical and systematic errors. For  $\alpha$  scattering, DIWS represents potential from density-independent single folding, while DDWS represents potential from density-dependent single folding.

Work	Model	$J^\pi = 2^+, 3^-$	
		$E_x = 1.29 \text{ MeV}$	$E_x = 2.27 \text{ MeV}$
		$B(E2)(e^2b^2)$	$B(E3)(e^2b^3)$
Present	DP	$0.229^{+0.007}_{-0.024}$	$0.116^{+0.003}_{-0.012}$
	DIF	$0.182^{+0.006}_{-0.019}$	$0.101^{+0.003}_{-0.011}$
	DDF	$0.233^{+0.007}_{-0.024}$	$0.133^{+0.004}_{-0.014}$
$\alpha$ scattering [43]	DP	$0.231 \pm 0.023$	$0.114 \pm 0.012$
	DIWS	$0.231 \pm 0.023$	$0.134 \pm 0.014$
	DDWS	$0.231 \pm 0.023$	$0.134 \pm 0.014$
$e$ scattering	EM	$0.229 \pm 0.015$	$0.120 \pm 0.015$
		[41]	[42]
	Adopted value	$0.209 \pm 0.006$	$0.132 \pm 0.018$
		[44]	[45]

There are two errors given for each fitted  $B(EL)$  value. The superscript one represents statistical error which comes from the fit of inelastic scattering cross sections and is about 3–4% of the fitted value. The subscript one represents the total error including both statistical error and systematic error which is about 10% of the fitted value.

The results are compared with  $B(EL)$  values obtained using electron inelastic scattering [41,42] and  $\alpha$  inelastic scattering [43], and also are compared with the adopted  $B(E2)$  [44] and  $B(E3)$  [45] values in Table III. The  $B(E2)$  and  $B(E3)$  values obtained with DP and DDF model in this work agree within errors with adopted values, and the values obtained from electron inelastic scattering and  $\alpha$  inelastic scattering. Past studies [25] have generally showed that  $B(EL)$  values obtained from inelastic scattering using folding calculations agreed with EM values, however, those obtained using DP calculation often do not, but for both the  ${}^6\text{Li}$  and  $\alpha$  experiments [43] on  ${}^{116}\text{Sn}$  the DP results agree well with the EM results. DIF model calculations do not agree with either adopted  $B(EL)$  values or  $B(EL)$  values obtained from electron scattering or  $\alpha$  scattering. Since the scattering process explored here is peripheral, lack of the density dependence for  $NN$  interaction may not be adequate to explain the discrepancy. The density used for the projectile in DIF calculation, a Fermi distribution obtained from the droplet model which gives a radius significantly smaller than the known  ${}^6\text{Li}$  radius [2], may not be suitable for the projectile since  ${}^6\text{Li}$  is a loosely bound light heavy ion.

## V. CONCLUSIONS

${}^6\text{Li}$  elastic scattering on  ${}^{116}\text{Sn}$  was studied with Woods-Saxon phenomenological potential model and double folding models with and without density dependence. For the angle

range measured in this experiment, from  $4^\circ \leq \theta_{\text{c.m.}} \leq 32^\circ$ , all the three models give good fits for the elastic scattering and cannot be distinguished. For folding models calculations, a renormalization factor  $N_R \sim 0.65$  is required to fit the elastic scattering data, consistent with earlier  ${}^6\text{Li}$  scattering studies. From Fig. 1, it seems another  $10^\circ$  larger angle measurement might help refine the parameters or determine which set of parameters are the best choice. The volume integral obtained with density dependent folding model using M3Y  $NN$  interaction is below Nadasen *et al.*'s prediction obtained with WS potential model, but agrees with Satchler's prediction obtained with S1Y  $NN$  interaction. The total reaction cross sections obtained from all the three models have less than 5% difference. Best fit  $B(EL)$  values for the low-lying  $2^+$  and  $3^-$  states with different models were obtained.  $B(EL)$  values obtained from deformed potential model calculations as well as from density dependent model calculations in this work agree well with adopted values and with those from electron inelastic scattering and  $\alpha$  inelastic scattering. The density independent folding model calculations do not reproduce the electromagnetic  $B(EL)$  values, which may indicate that density choice for projectile is not suitable.

## ACKNOWLEDGMENTS

We thank Dr. Florin Carstoiu and Dr. Livius Trache for their help and providing computer code in density independent folding calculations. We also thank Dr. D. T. Khoa and Mr. Hoang Sy Than for their help and providing the computer codes to do the CDM3Yn folding calculations and cross section calculations. This work was supported in part by the US Department of Energy under Grant No. DE-FG02-93ER40773 and by the Robert A. Welch Foundation under Grant A-0558.

- 
- [1] D. H. Youngblood, H. L. Clark, and Y.-W. Lui, Nucl. Phys. **A649**, 49c (1999).
  - [2] G. Satchler and W. G. Love, Phys. Rep. **55**, 183 (1979).
  - [3] M. Branden and G. Satchler, Phys. Rep. **285**, 143 (1997).
  - [4] Y. Sakuragi, M. Yahiro, and M. Kamimura, Prog. Theor. Phys. Suppl. **89**, 136 (1986).
  - [5] Y. Sakuragi, Phys. Rev. C **35**, 2161 (1987).
  - [6] Y. Sakuragi, M. Ito, Y. Hirabayashi, and C. Samanta, Prog. Theor. Phys. **98**, 521 (1997).
  - [7] R. M. DeVries, D. A. Goldberg, J. W. Watson, M. S. Zisman, and J. G. Cramer, Phys. Rev. Lett. **39**, 450 (1977).
  - [8] M. E.-A. Farid and M. A. Hassanain, Nucl. Phys. **A678**, 39 (2000).
  - [9] H. G. Bingham, M. L. Halbert, D. C. Hensley, E. Newman, K. W. Kemper, and L. A. Charlton, Phys. Rev. C **11**, 1913 (1975).
  - [10] J. E. Poling, E. Norbeck, and R. R. Carlson, Phys. Rev. C **13**, 648 (1976).
  - [11] L. T. Chua, F. D. Becchetti, J. Jänecke, and F. L. Milder, Nucl. Phys. **A273**, 243 (1976).
  - [12] P. Schwandt, W. W. Jacobs, M. D. Kaitchuck, P. P. Singh, W. D. Plouffe, F. D. Becchetti, and J. Jänecke, Phys. Rev. C **24**, 1522 (1981).
  - [13] S. Micek, Z. Majka, H. Rebel, H. J. Gils, and H. Klewe-Nebenius, Nucl. Phys. **A435**, 621 (1984).
  - [14] A. C. Demijanov, V. N. Bragin, A. A. Ogloblin, A. L. Lebedev, J. M. Bang, S. A. Goncharov, S. N. Ershov, F. A. Gareev, and P. P. Korovin, Phys. Lett. **B184**, 129 (1987).
  - [15] A. Nadasen, M. McMaster, G. Gunderson, A. Judd, S. Villanueva, P. Schwandt, J. S. Winfield, J. van der Plicht, R. E. Warner, F. D. Becchetti *et al.*, Phys. Rev. C **37**, 132 (1988).
  - [16] A. Nadasen, M. McMaster, M. Fingal, J. Tavormina, P. Schwandt, J. S. Winfield, M. F. Mohar, F. D. Becchetti, J. W. Jänecke, and R. E. Warner, Phys. Rev. C **39**, 536 (1989).
  - [17] A. Nadasen, T. Stevens, J. Farhat, J. Brusoe, P. Schwandt, J. S. Winfield, G. Yoo, N. Anantaraman, F. D. Becchetti, J. Brown *et al.*, Phys. Rev. C **47**, 674 (1993).
  - [18] K. Schwarz, C. Samanta, M. Fujiwara, H. Rebel, R. De Leo, N. Matsuoka, H. Utsunomiya, H. Akimune, I. Daito, H. Fujimura *et al.*, Eur. Phys. J. A **7**, 367 (2000).
  - [19] D. H. Youngblood, Y.-W. Lui, and H. L. Clark, Phys. Rev. C **60**, 014304 (1999).
  - [20] D. H. Youngblood and J. D. Bronson, Nucl. Instrum. Methods A **361**, 37 (1995).

- [21] D. M. Pringle, W. N. Catford, J. S. Winfield, D. G. Lewis, N. A. Jelley, K. W. Allen, and J. H. Coupland, Nucl. Instrum. Methods A **245**, 230 (1986).
- [22] D. H. Youngblood, Y.-W. Lui, H. L. Clark, P. Oliver, and G. Simler, Nucl. Instrum. Methods A **361**, 539 (1995).
- [23] D. H. Youngblood, Y.-W. Lui, and H. L. Clark, Phys. Rev. C **55**, 2811 (1997).
- [24] G. R. Satchler, *Direct Nuclear Reactions* (Oxford University Press, New York, 1983).
- [25] J. R. Beene, D. J. Horen, and G. R. Satchler, Phys. Rev. C **48**, 3128 (1993).
- [26] J.-P. Jeukenne, A. Lejeune, and C. Mahaux, Phys. Rev. C **16**, 80 (1977).
- [27] G. Satchler, Nucl. Phys. **A579**, 241 (1994).
- [28] G. Bertsch, J. Borysowicz, H. McManus, and W. G. Love, Nucl. Phys. **A284**, 399 (1977).
- [29] M. Lacombe, B. Loiseau, J. M. Richard, R. Vinh. Mau, J. Côté, P. Pirès, and R. de Tournel, Phys. Rev. C **21**, 861 (1980).
- [30] W. G. Love and L. W. Owen, Nucl. Phys. **A239**, 74 (1975).
- [31] D. T. Khoa and W. von Oertzen, Phys. Lett. **B304**, 8 (1993).
- [32] D. T. Khoa, G. R. Satchler, and W. von Oertzen, Phys. Rev. C **56**, 954 (1997).
- [33] D. T. Khoa and G. R. Satchler, Nucl. Phys. **A668**, 3 (2000).
- [34] F. Carstoiu (unpublished).
- [35] G. R. Satchler, Nucl. Phys. **A472**, 215 (1987).
- [36] A. A. Korshennikov, E. Y. Nikolskii, C. A. Bertulani, S. Fukuda, T. Kobayashi, E. A. Kuzmin, S. Momota, B. G. Novatskii, A. A. Ogloblin, and E. A. A. Ozawa, Nucl. Phys. **A617**, 45 (1997).
- [37] J. Raynal, ECIS code, (unpublished); J. Raynal, Proceedings of the Workshop on Applied Nuclear Theory and Nuclear Model Calculations for Nuclear Technology Application, Trieste, Italy, 1988.
- [38] G. R. Satchler and D. T. Khoa, Phys. Rev. C **55**, 285 (1997).
- [39] D. T. Khoa (unpublished); D. T. Khoa and G. R. Satchler, Nucl. Phys. **A668**, 3 (2000).
- [40] S. Gupta and K. Murthy, Z. Phys. A **307**, 187 (1982).
- [41] J. W. Lightbody, S. Penner, S. P. Fivozinsky, P. L. Hollowell, and H. Crannell, Phys. Rev. C **14**, 952 (1976).
- [42] P. Barreau and J. B. Bellicard, Phys. Rev. Lett. **19**, 1444 (1967).
- [43] H. L. Clark, Y.-W. Lui, and D. H. Youngblood, Phys. Rev. C **57**, 2887 (1998).
- [44] S. Raman, C. W. Nestor, Jr., and P. Tikkanen, At. Data Nucl. Data Tables **78**, 1 (2001).
- [45] T. Kibédi and R. H. Spear, At. Data Nucl. Data Tables **80**, 35 (2002).